### Title

Measurement of bound and pore water T1 relaxation times in cortical bone using three-dimensional ultrashort echo time cones sequences




### Journal

Magnetic Resonance in Medicine, 77(6)

### ISSN

0740-3194



### Authors

Chen, Jun
Chang, Eric Y
Carl, Michael
et al.



### Publication Date

2017-06-01

### DOI

10.1002/mrm.26292

# Measurement of Bound and Pore Water $T_1$ Relaxation Times in Cortical Bone Using Three-Dimensional Ultrashort Echo Time Cones Sequences

Jun Chen,[1,2] Eric Y. Chang,[1,3] Michael Carl,[4] Yajun Ma,[1] Hongda Shao,[1] Bimin Chen,[1] Zhihong Wu,[2] and Jiang Du[1]*

**Purpose:** We present three-dimensional ultrashort echo time Cones (3D UTE Cones) techniques for quantification of total water $T_1$ ($T_1^{TW}$), bound water $T_1$ ($T_1^{BW}$), and pore water $T_1$ ($T_1^{PW}$) in vitro and in vivo using a 3 Tesla (T) scanner.

**Methods:** $T_1^{TW}$, $T_1^{BW}$, and $T_1^{PW}$ were measured with three-dimensional (3D) Cones and adiabatic inversion recovery Cone (IR-Cone) sequences. Two-dimensional (2D) nonselective ultrashort echo time (UTE) techniques, including saturation recovery, variable repetition times (TRs), and inversion recovery (IR) preparation approaches were compared with 3D-Cones techniques on bovine cortical bone samples ($n = 8$). The 3D Cones sequences were used to measure $T_1^{TW}$, $T_1^{BW}$, and $T_1^{PW}$ in the tibial midshaft of healthy volunteers ($n = 8$).

**Results:** Comparable $T_1$ images were achieved for cortical bone between 3D Cones and 2D UTE techniques as well as those published in the literature. The 3D Cones sequences showed a mean $T_1^{TW}$ of $208 \pm 22$ ms, a mean $T_1^{PW}$ of $545 \pm 28$ ms, and a mean $T_1^{BW}$ of $131 \pm 12$ ms for bovine cortical bone; and a mean $T_1^{TW}$ of $246 \pm 32$ ms, a mean $T_1^{PW}$ of $524 \pm 46$ ms, and a mean $T_1^{BW}$ of $134 \pm 11$ ms for the tibial midshaft of healthy volunteers.

**Conclusions:** The 3D Cones sequences can be used for fast volumetric assessment of bound and pore water $T_1$ images in vitro and in vivo. **Magn Reson Med 77:2136–2145, 2017.** 

**Key words:** cortical bone; UTE; Cones; bound water; pore water; $T_1$ measurement

## INTRODUCTION

Osteoporosis is defined by decreased bone strength (1) and is characterized by thinning and increased porosity of cortical bone as well as architectural deterioration of trabecular bone (2–5). Cortical bone is particularly important, as approximately 80% of the skeleton and approximately 80% of all fractures associated with advanced age arise at sites that are composed primarily of cortical bone (6). Cortical bone has a hierarchical physical structure (7) and consists of mineral (~43% by volume), organic matrix (~35%), and water (~22%) (8,9). The water exists in various locations and in different states, including water bound to the organic matrix (bound water (BW)) and water residing in Haversian canals and in lacunae-canalicular systems (pore water (PW)) (9–14). Bound and pore water pools show opposite correlations with biomechanical measures of bone competence (15,16). Therefore, it is of critical importance to develop techniques to noninvasively evaluate properties of cortical bone, including bound and pore water components.

Magnetic resonance (MR) imaging is uniquely suited for imaging of water. However, cortical bone water has a short $T_2^*$, which can barely be detected by conventional clinical MR sequences (17). Ultrashort echo time (UTE) techniques have been used to acquire signal from cortical bone water before it decays to zero or near-zero levels. Using UTE-based techniques, total bone water (including both bound water and pore water) $T_1$ ($T_1^{TW}$) and concentration can be measured using clinical MR scanners (18–20). Furthermore, bound and pore water $T_2^*$ images and relative fractions can be accessed using bi-exponential fitting of UTE signal decay (19–23). Bound water $T_2^*$ images can be measured selectively with adiabatic inversion recovery prepared UTE (IR-UTE) techniques in which pore water with a longer $T_2^*$ can be selectively suppressed (24). However, $T_1$ of bound water ($T_1^{BW}$) and pore water ($T_1^{PW}$) have not been well investigated using clinical MR scanners, although $T_1^{BW}$ and $T_1^{PW}$ have been reported using high-performance NMR spectrometers (22,25). Accurate measurement of bound and pore water concentrations require compensation of $T_1$ and $T_2^*$ effects (25–27). Reliability and fast measurements of $T_1^{BW}$ and $T_1^{PW}$ would also be necessary to be performed in vivo in the clinical setting.

The three-dimensional (3D) Cones UTE sequence employs a short radio frequency (RF) rectangular pulse for signal excitation, followed by 3D spiral trajectories sampled on the Cones (28,29). The Cones sequence provides 3D volumetric UTE imaging in a time-efficient way with greatly reduced eddy current artifacts compared with the regular two-dimensional (2D) slice-selective UTE sequence. Our previous studies have shown that the 2D spiral UTE sequence has improved signal-to-noise (SNR) efficiency compared with the 2D radial UTE sequence (30). The 3D Cones sequence is expected to have further improved SNR efficiency compared with the 2D spiral UTE sequence as well as the 2D or 3D radial UTE sequences (30,31). The purpose of this study

[1]Department of Radiology, University of California, San Diego, California, USA.

[2]Department of Orthopedics, Peking Union Medical College, Beijing, China.

[3]Radiology Service, VA San Diego Healthcare System, San Diego, California, USA.

[4]Applied Science Lab, GE Healthcare, San Diego, California, USA

*Correspondence to: Jiang Du, PhD, Department of Radiology, University of California, San Diego, 200 West Arbor Drive, San Diego, CA 92103-8226. Telephone: (619) 471-0519; Fax: (619) 471-0503;
E-mail: jiangdu@ucsd.edu.

Received 6 January 2016; revised 29 April 2016; accepted 7 May 2016

DOI 10.1002/mrm.26292

Published online 6 June 2016 in Wiley Online Library (wileyonlinelibrary.com).

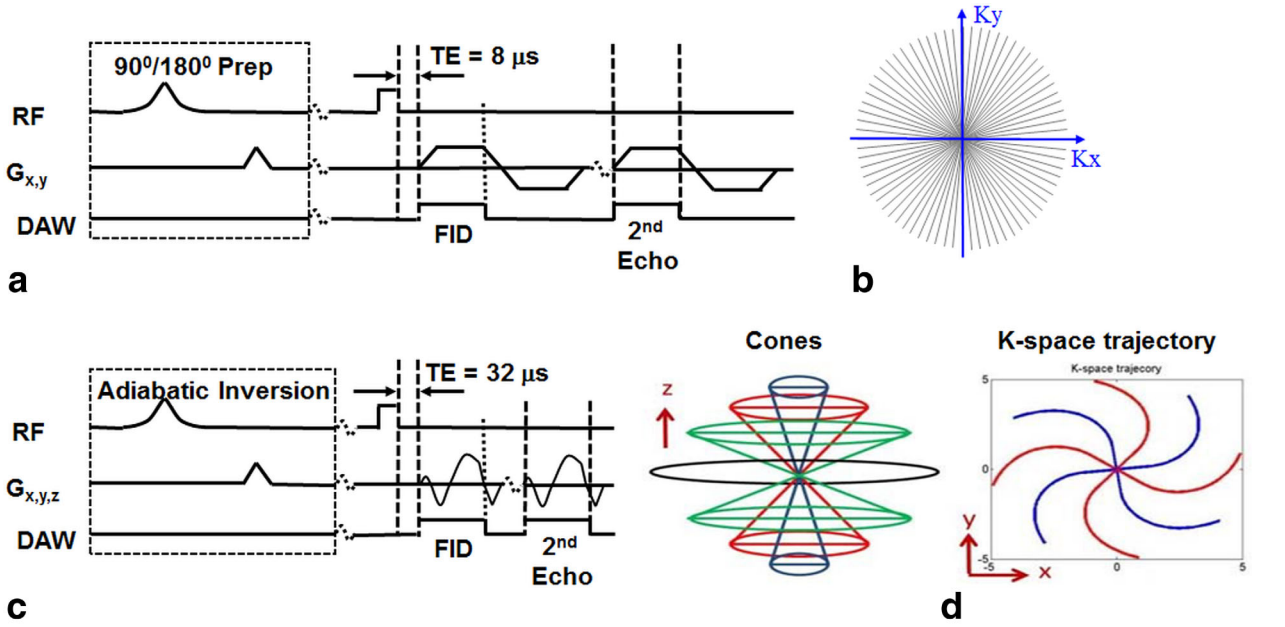


FIG. 1. The 2D non-slice-selective UTE (a) and 3D UTE Cones (c) sequences, as well as sampling trajectories for 2D UTE (b) and 3D Cones (d). Both the 2D UTE and 3D Cones sequences employ a short rectangular pulse (duration = 26–52 μs) for signal excitation followed by single or dual-echo radial ramp sampling. Magnetization preparation including short 90° saturation pulse (duration = 248 μs) and long adiabatic inversion pulse (duration = 8.64 ms) can be applied before UTE data acquisitions.

was to use the efficient 3D-Cones sequences for fast volumetric measurement of $T_1^{BW}$ and $T_1^{PW}$ of cortical bone in vitro and in vivo. Comparison studies between 2D UTE and 3D Cones sequences were performed on a rubber phantom and ex vivo bovine bone samples. Finally, the 3D Cones techniques were applied to healthy volunteers on a 3 Tesla (T) scanner to demonstrate the feasibility of fast volumetric assessment of $T_1^{BW}$ and $T_1^{PW}$ in vivo.

## METHODS

### Sample Preparation

Eight bovine cortical bone samples were harvested from mature bovine femoral midshafts obtained from a local slaughterhouse, and were cleared of external muscle and soft tissue. Bone marrow was removed with a scalpel. Cross-sectional cortical bone segments with an approximate thickness of 60 mm were sectioned using a low-speed diamond saw (Isomet 1000, Buehler, Bluff, Illinois) with constant saline irrigation, and stored in phosphate buffered saline (PBS) solution for 24 h prior to use. A piece of rubber (Pink Eraser, Paper Mate Products, Newell Brands, Atlanta, GA) was used as a reference phantom for $T_1$ quantification (details shown below).

### Pulse Sequences

Figure 1 shows the 3D Cones UTE sequences as well as previously reported 2D radial UTE sequences implemented on a 3T Signa TwinSpeed scanner (GE Healthcare Technologies, Milwaukee, Wisconsin). The basic 3D Cones sequence (Fig. 1c) employed a short RF rectangular pulse (duration = 26–52 μs) for signal excitation, followed by 3D spiral trajectories sampled on the Cones (Fig. 1d) (29). The Cones sequence provides 3D volumetric UTE imaging in a time-efficient way with eddy current artifacts greatly reduced over the regular 2D UTE sequence, which employs half-pulses for selective excitation and thus are sensitive to eddy currents and gradient errors (32). To minimize sensitivity to eddy currents, we used 2D non-slice-selective UTE rather than slice-selective UTE sequences (Fig. 1a), in which the slice-selective half-pulse excitation was replaced with a short rectangular pulse (duration = 26–52 μs). This eliminates the eddy currents while offering much improved SNR caused by projection imaging in the slice dimension. The nonselective UTE imaging also speeds up data acquisition, as only one excitation is needed (2D slice-selective imaging requires two excitations). The 2D nonselective UTE sequences are used to compare the 3D Cones UTE sequences in $T_1$ analysis of bound and pore water components in bovine cortical bone samples.

Both bound and pore water are detectable with the basic 2D radial UTE and 3D Cones UTE sequences. The UTE sequences can also be combined with an adiabatic inversion recovery preparation pulse (Silver-Hoult pulse with duration of 8.64 ms, spectral bandwidth of 1.5 kHz) for IR-Cones or IR-UTE imaging of bound water (29). The purpose of the adiabatic IR pulse is to invert the longitudinal magnetization of the long $T_2$ signal components, including those in muscle and fat as well as pore water (25,33). The magnetization of collagen-bound water, which has a very short $T_2^*$, is not inverted but is largely saturated by the adiabatic IR pulse (25). After an inversion time (TI) delay, during which the inverted pore water magnetization approaches the null point, the Cones acquisition is initiated to selectively detect signal from collagen-bound water. To speed up data acquisition, one IR preparation is followed by five Cones sampling (29).

### $T_1^{TW}$ and $T_1^{PW}$ Measurement with Saturation Recovery UTE (SR-UTE)

Saturation recovery UTE (SR-UTE) has been employed for $T_1$ measurement of cortical bone (33). In this technique, a $90^0$ rectangular pulse (duration = 232 μs) was devised in conjunction with large dephasing gradients to suppress signals from both long and short $T_2$ species. UTE acquisition started at a series of saturation recovery time (TSR) to detect the signal recovery from bone. Only the 2D nonselective UTE sequence was combined with the short 90° rectangular pulse for SR-UTE imaging. The 3D Cones sequence was not combined with the SR approach, as a result of excessively lengthy scan times. The single exponential signal recovery model shown below was used to fit $T_1$ (18,33):

$$S(TSR, TE = 8\mu s) = S_0 \times [1 - (1 - k) \times e^{-TSR/T_1^{TW}}] + C \quad [1]$$

where S(TSR,TE=8 μs) is the UTE-TSR signal intensity, $S_0$ is the steady-state UTE signal intensity, $k$ accounts for the residual fraction of the longitudinal magnetization of cortical bone after a nominal 90° pulse, $T_1^{TW}$ is the effective $T_1$ of bone water with signal contribution from both bound and pore water in cortical bone.

Bound-water signal has an extremely short $T_2^*$ of approximately ~300 μs, whereas pore water has a much longer $T_2^*$ of several milliseconds. Therefore, a longer TE (eg, TE = 2.5 ms) can be used to selectively detect signal from pore water with near-zero signal contribution from bound water. In this case, SR-UTE can be used to measure $T_1$ of pore water ($T_1^{PW}$) based on the following equation:

$$S(TSR, TE = 2.5ms) = S_0 \times [1 - (1 - k) \times e^{-TSR/T_1^{PW}}] + C \quad [2]$$

Each bovine cortical bone sample was placed in Fomblin solution, which helped in maintaining the hydration of cortical bone and minimizing the susceptibility effects at tissue-air interfaces. A wrist coil (BC-10, Medspira, Minneapolis, Minnesota) was used for signal excitation and reception. The 2D dual-echo SR-UTE sequence employed the following imaging parameters for $T_1$ quantification: field of view (FOV) = 15 cm, sampling bandwidth (BW) = 125 kHz, flip angle = 20°, TE = 8 μs and 2.5 ms, TR = 1000 ms, eight SR-UTE acquisitions (TSRs = 7, 25, 50, 100, 200, 400, 600, 800 ms), reconstruction matrix size = 256 × 256, in-plane pixel size = 0.31 × 0.31 $mm^2$, scan time = 28 min.

### $T_1^{TW}$ and $T_1^{PW}$ Measurement With UTE Variable TR (UTE-VTR) Approach

The steady-state UTE signal $S^{UTE}$ can be written as (18):

$$S^{UTE} \propto S_0^{UTE} \times f_{xy}(B_1(t), T_1, T_2) \times (1 - e^{-TR/T_1}) \times e^{-TE/T_2^*} / (1 - f_z(B_1(t), T_1, T_2) \times e^{-TR/T_1})) \quad [3]$$

where $f_{xy}$ and $f_z$ describe the behavior of the transverse magnetization and longitudinal magnetization, respectively, as a function of the pulse $B_1(t)$ as well as the $T_2$ and $T_1$ of the ultrashort $T_2^*$ components, and $S_0^{UTE}$ is the UTE signal with full longitudinal recovery. For both the 2D nonselective UTE and 3D Cones UTE sequences, the duration of the excitation pulse (ie, 52 μs, 20° rectangular pulse) is significantly shorter than both $T_2$ and $T_1$ of bone water; therefore, relaxation effects during RF excitation could be ignored as a first-order approximation. Therefore, this equation can be simplified as follows:

$$S^{UTE}(TR, TE = 8\mu s) = S_0^{UTE} \times f_{xy} \times (1 - e^{-TR/T_1^{TW}}) \times e^{-TE/T_2^{*TW}} / (1 - f_z \times e^{-TR/T_1^{TW}})) \quad [4]$$

where $T_2^{*TW}$ is the effective $T_2^*$ of bound and pore water in cortical bone.

When a longer echo time (TE) is used, bound water signal decays to near zero and only pore water is detected. As a result, $T_1^{PW}$ can be measured selectively with UTE-VTR acquisitions with a longer TE (eg, 2.5 ms). Pore water $T_1$ can then be measured with the following equation [34]:

$$S^{UTE}(TR, TE = 2.5ms) = S_{0,}^{UTE} \times f_{xy} \times (1 - e^{-TR/T_1^{PW}}) \times e^{-TE/T_2^{*PW}} / (1 - f_z \times e^{-TR/T_1^{PW}})) \quad [5]$$

Because only pore water is detected with a TE of 2.5 ms, $T_2^{*PW}$ should be used in this equation.

The following bicomponent model was used to quantify the $T_2^*$ and relative fractions of bound and pore water components in cortical bone (13):

$$SI(TE) = S^{BW} \times e^{-TE/T_2^{*BW}} + S^{PW} \times e^{-TE/T_2^{*PW}} + \text{noise} \quad [6]$$

where $S^{BW}$ and $S^{PW}$ are the corresponding signal intensities of bound and pore water components at TE of 0.

The experimental setup was similar to that used in the SR-UTE approach. The dual-echo 2D nonselective UTE-VTR technique employed similar imaging parameters except eight pulse repetition times (TRs) of 14, 25, 50, 100, 200, 400, 600, and 800 ms, and a total scan time of 12 min. The dual-echo 3D Cones-VTR technique employed similar imaging parameters except 10 slices, a slice thickness of 7 mm, nine TRs of 6, 10, 15, 20, 25, 30, 50, 100, and 200 ms, 280 sampling points per Cones trajectory (sampling window = 1120 μs, spiral trajectories = 3728), and a total scan time of 28 min. $T_2^*$ was measured with single-echo 2D UTE and 3D Cones with 15 TEs (TEs = 8 or 32 μs, 0.1, 0.2, 0.3, 0.4, 0.6, 0.8, 1, 1.5, 2, 3, 4, 6, 8, and 10 ms), and a constant TR of 100 ms for 2D UTE and 20 ms for 3D Cones. The total scan time for $T_2^*$ quantification was 6 min for 2D UTE and 19 min for 3D Cones.

### $T_1^{BW}$ Measurement with IR-UTE Variable TR/TI Approach

In IR-UTE, the long $T_2$ signal from pore water is inverted and nulled, while the short $T_2$ signal from bound water is saturated and recovered during the inversion time of TI, and subsequently detected by UTE data acquisitions. The steady-state IR-UTE signal following an adiabatic IR pulse can be calculated as follows (35):

$$S^{IR-UTE}(TR, TI, TE = 8\mu s) = S_0^{IR-UTE} \times [1 + (Q-1) \times e^{-TI/T_1^{BW}} - Q \times e^{-TR/T_1^{BW}}]/ (1 - Q \times f_z \times e^{-TR/T_1^{BW}}) \quad [7]$$

where $S_0^{IR-UTE}$ is the steady state IR-UTE signal of cortical bone, and $Q$ is the fraction of longitudinal magnetization of bound water following the adiabatic IR pulse. Our previous studies suggest that bound water $T_2^*$ is approximately ~0.3 ms, yielding a $Q$ value of less than 0.05 following Bloch equation simulation. This near-complete saturation of bound-water component is consistent with results reported by other groups (25–27,36). As a result, Eq. [7] can be simplified as follows (35):

$$S^{IR-UTE}(TR, TI, TE = 8\mu s) \propto S_0^{IR-UTE} \times (1 - e^{-TI/T_1^{BW}}) \quad [8]$$

Eq. [8] suggests that $T_1$ of bound water can be measured reliably using exponential fitting of IR-UTE images acquired with different combinations of TR and TI, on the condition that all of these TR/TI combinations satisfy the nulling of pore water in cortical bone. Although TR is not shown explicitly in Eq. [8], varying TI is associated with varying TR, as TI depends on TR in the nulling condition (35).

The experimental setup was similar to those used in the SR-UTE and UTE-VTR approaches. The 2D nonselective IR-UTE sequence employed similar imaging parameters except the reduced reconstruction matrix size of $128 \times 128$, five TR/TI combinations (representative TR/TI values = 50/24; 100/48; 200/90; 300/130, and 400/160 ms, in which TI was adjusted based on the measured $T_1^{PW}$ and was further verified by measuring the decay of IR-UTE signals, and a total scan time of 6 min). A single-component $T_2^*$ signal decay would suggest the nulling of pore water and selective detection of bound water (24). The 3D IR-Cones UTE sequence employed similar imaging parameters except reconstruction matrix size = $128 \times 128 \times 10$, a slice thickness of 7 mm, the same five TR/TI combinations, and a total scan time of 10 min. $T_2^*$ was measured with 2D IR-UTE and 3D IR-Cones sequences, respectively, with 15 TEs (TEs = 8 or 32 μs, 0.1, 0.2, 0.3, 0.4, 0.6, 0.8, 1, 1.5, 2, 3, 4, 6, 8, and 10 ms), and a total scan time of 90 min for 2D IR-UTE and 150 min for 3D IR-Cones imaging, respectively.

### $T_1$ Measurements In Vivo

The 3D Cones and IR-Cones sequences were applied to the tibial midshaft of eight healthy volunteers (all males, 27–42 years old, mean/standard deviation = 32 ± 5) for bound and pore water $T_1$ measurements in vivo. Written, informed consent approved by our Institutional Review Board was obtained before their participation in this study. An eight-channel knee coil was used for signal excitation and reception.

To measure $T_1^{TW}$ and $T_1^{PW}$, the following dual-echo 3D Cones-VTR imaging parameters were used for in vivo studies: FOV = 15 cm, BW = 250 kHz, flip angle = 18°, TE = 32 μs and 2.5 ms, 10 slices, slice thickness = 7 mm, five TRs of 7.8, 11, 15, 20 and 30 ms, reconstruction matrix size = $192 \times 192$, scan time = 14 min. To measure $T_1^{BW}$, the following 3D IR-Cones imaging parameters were used for in vivo studies: FOV = 15 cm, BW = 250 kHz, flip angle = 18°, TE = 32 μs, 10 slices, slice thickness = 7 mm, five TR/TI combinations (representative TR/TI values = 50/24; 100/48; 200/90; 300/130; 400/160 ms). TI was adjusted based on the measured $T_1^{PW}$, reconstruction matrix size = $128 \times 128 \times 10$, scan time = 11 min.

### Data Analysis

The analysis algorithm was written in MATLAB (The MathWorks, Natick, Massachusetts) and was executed offline on the DICOM images obtained by the protocols described previously. The program allowed placement of regions of interest (ROIs) on the first UTE image of the series, which was then copied onto each of the subsequent images. The mean intensity within each of the ROIs (approximately 50 pixels) was used for subsequent curve fitting. $T_1^{TW}$ was estimated using Eq. [1] for the SR-UTE approach, and Eq. [4] for the UTE acquisitions with variable TR approach. $T_1^{PW}$ was estimated using Eq. [2] for the SR-UTE approach, and Eq. [5] for the UTE acquisitions with variable TR approach. $T_1^{BW}$ was estimated using Eq. [8] for the IR-UTE approach (TI was calculated for each TR based on the measured $T_1^{PW}$). Bicomponent $T_2^*$ analysis was performed on 2D UTE and 3D Cones as well as 2D IR-UTE and 3D IR-Cones images using Eq. [6]. The estimated results of $T_1^{TW}$, $T_1^{PW}$, and $T_1^{BW}$ were compared between nonselective 2D UTE and 3D Cones sequences in the bovine bone study. Then the 3D Cones and IR-Cones techniques were applied to healthy volunteers with mean and standard deviation of calculated $T_1^{TW}$, $T_1^{PW}$, and $T_1^{BW}$. The SNR was introduced to evaluate the efficiency of 3D Cones and IR-Cones UTE imaging of cortical bone in vivo. SNR was calculated by dividing the mean signal intensity measured in cortical bone by the noise measured in air.

## RESULTS

Figure 2 shows representative dual echo 2D SR-UTE, 2D UTE-VTR, and 3D Cones-VTR images of a bovine cortical bone sample, as well as bicomponent fitting of $T_2^*$ data, and single-component fitting of $T_1$ data from a representative ROI drawn in cortical bone and rubber phantom, respectively. Two distinct $T_2^*$ components were observed in cortical bone, while a single component was observed in the rubber eraser. $T_1^{TW}$, $T_1^{PW}$, and $T_1^{BW}$ values derived from all three techniques were largely consistent for both the cortical bone and the rubber eraser, as noted in the figure.

Figure 3 shows representative 2D IR-UTE and 3D IR-Cones images of the same bovine cortical bone sample, as well as bicomponent fitting of $T_2^*$ data and single-component fitting of $T_1$ data from the same ROI. Both bicomponent fitting and single-component fitting of IR-UTE and 3D IR-Cones images show similar results with a single $T_2^*$ of ~0.25 ms, which is similar to the short $T_2^*$ value derived from the bicomponent fitting of 2D UTE and 3D Cones imaging. The same single component $T_2^*$ decay behavior was observed with different TR and TI combinations in 2D IR-UTE and 3D IR-Cones imaging of all bone samples. These results demonstrate that pore

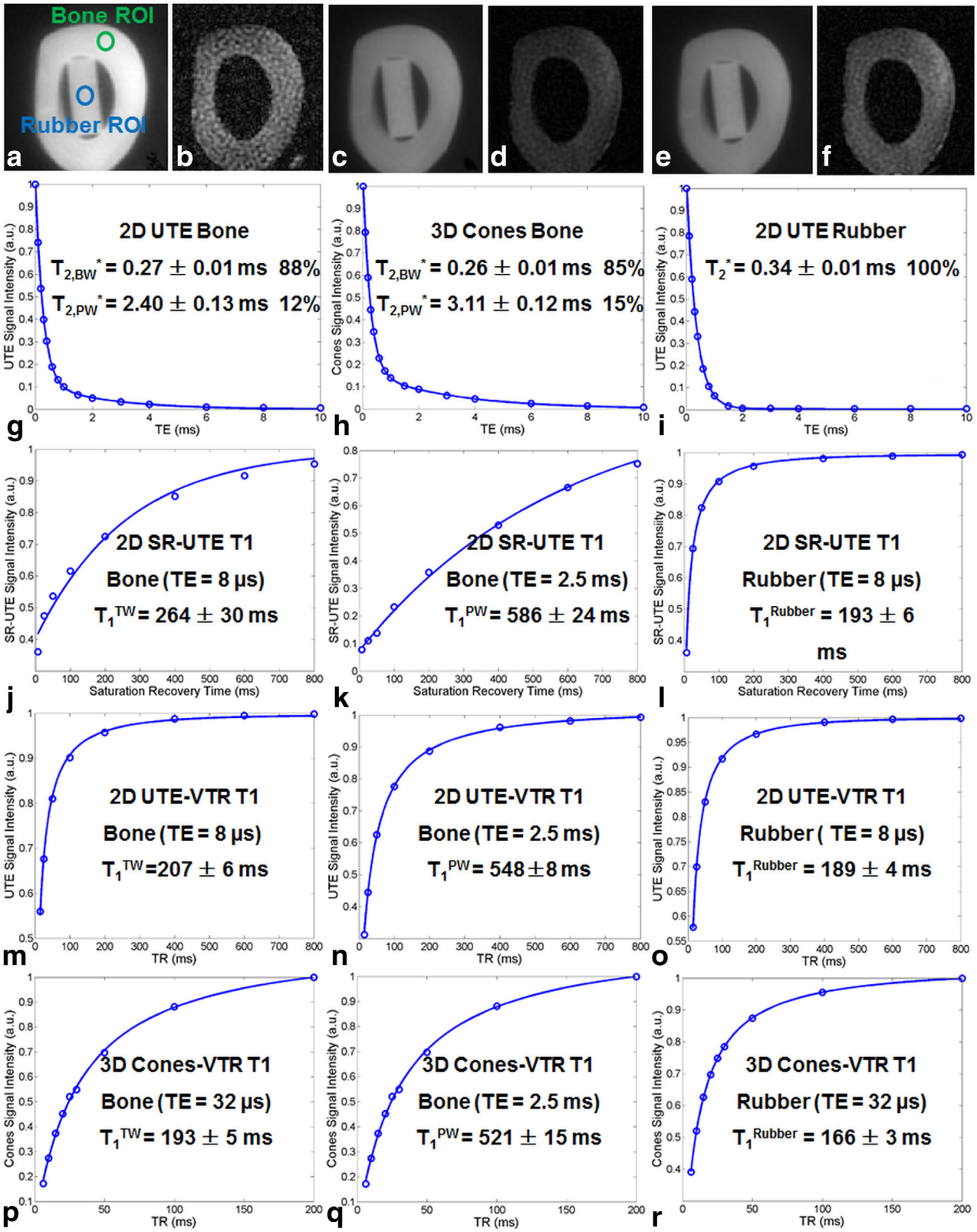


FIG. 2. Selected images of a bovine cortical bone sample acquired with 2D dual echo saturation recovery UTE with a TSR of 100 ms, TEs of 8 μs (a) and 2.5 ms (b), 2D dual echo UTE with a TR of 100 ms and TEs of 8 μs (c) and 2.5 ms (d), and 3D dual echo Cones with a TR of 20 ms and TEs of 8 μs (e) and 2.5 ms (f). Both 2D UTE (g) and 3D Cones (h) show similar bicomponent $T_2^*$ decay for cortical bone (bound water with a shorter $T_2^*$ of 0.26/0.27 ms and pore water with a longer $T_2^*$ of 2.40/3.11 ms) and single-component $T_2^*$ decay for rubber (i). Single-component exponential recovery curve fitting shows a $T_1^{TW}$ of 264 ± 30 ms (j), a $T_1^{PW}$ of 586 ± 24 ms (k), and a $T_1^{rubber}$ of 193 ± 6 ms (l) with the SR-UTE approach, a $T_1^{TW}$ of 207 ± 6 ms (m), a $T_1^{PW}$ of 548 ± 8 ms (n), and a $T_1^{rubber}$ of 185 ± 4 ms (o) with the UTE-VTR approach, and a $T_1^{TW}$ of 193 ± 5 ms (p), a $T_1^{PW}$ of 521 ± 15 ms (q), and a $T_1^{rubber}$ of 166 ± 3 ms (r).

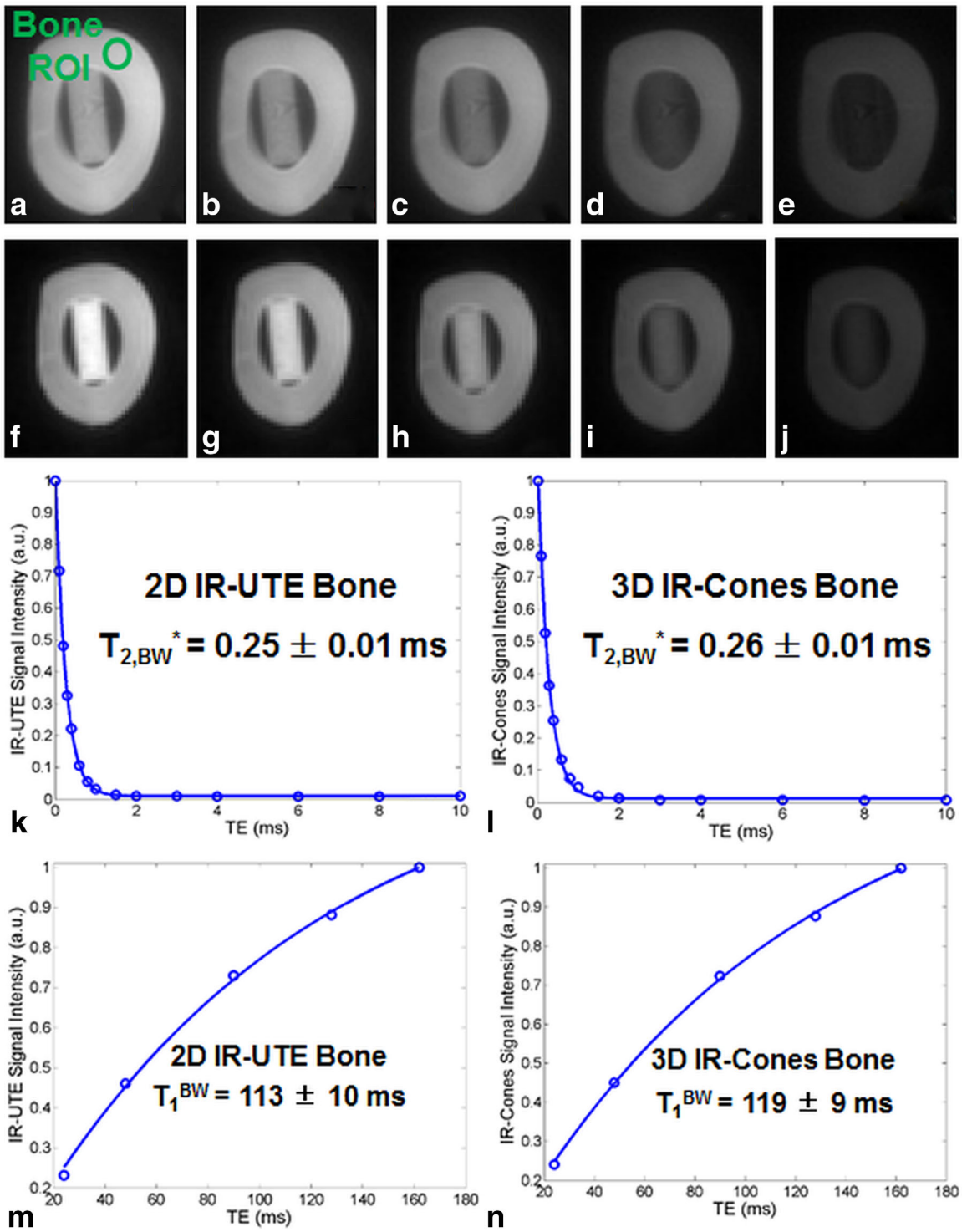


FIG. 3. Two-dimensional IR-UTE imaging of a bovine cortical bone sample with a series of TR/TI combinations of 400/164 ms (a), 300/129 ms (b), 200/91 ms (c), 100/48 ms (d), 50/24 ms (e), and 3D IR-Cones imaging with the same TR/TI combinations of 400/164 ms (f), 300/129 ms (g), 200/91 ms (h), 100/48 ms (i), and 50/24 ms (j). Excellent single-component fitting of images acquired with different TEs was achieved for cortical bone with a $T_2^{*BW}$ of 0.25 ± 0.01 ms derived from 2D IR-UTE images (k) and a $T_2^{*BW}$ of 0.26 ± 0.01 ms derived from 3D IR-Cones images (l). Exponential fitting of images acquired with different TR/TI combinations was achieved for cortical bone with a $T_1^{BW}$ of 113 ± 10 ms derived from 2D IR-UTE images (m) and a $T_1^{BW}$ of 119 ± 9 ms derived from 3D IR-Cones images (n).

water with longer $T_2^*$ images was suppressed, and bound water with much shorter $T_2^*$ was selectively imaged. $T_1^{BW}$ from the 3D IR-Cones approach (119 ± 9 ms) is comparable to that of 113 ± 10 ms from the 2D IR-UTE approach.

Table 1 provides the mean and standard deviation of $T_1^{TW}$, $T_1^{PW}$, and $T_1^{BW}$. All of the measurements were consistent between the different techniques. $T_1$ values from the literature were also summarized. Our measurements

Table 1
Measurement of $T_1$ Values of Pore Water ($T_1^{PW}$), Bound Water ($T_1^{BW}$), and Total Water ($T_1^{TW}$) in Bovine Cortical Bone (n = 8) Using 2D Nonselective Saturation Recovery UTE (SR-UTE), 2D UTE With Variable TRs, 2D IR-UTE With Variable TR and TI Combinations, 3D UTE Single-Echo Cones With Variable TRs, 3D Dual Echo Cones With Variable TRs, and 3D IR-Cones With Variable TR and TI Combinations, Respectively.

| Authors | Field Strength | Sequences | Pore Water $T_1$, ($T_1^{PW}$, ms) | Bound Water $T_1$ ($T_1^{BW}$, ms) | Total Water $T_1$, ($T_1^{TW}$, ms) |
|---|---|---|---|---|---|
| Chenet al. | 3T | 2D dual-echo SR-UTE | 574 + 36 | - | 256 + 28 |
| Chenet al. | 3T | 2D dual-echo UTE-VTR | 560 ± 32 | - | 214 ± 25 |
| Chenet al. | 3T | 2D IR-UTE Variable TR/T1 | - | 122 ± 9 | - |
| Chenet al. | 3T | 3D dual-echo Cones-VTR | 545 ± 28 | - | 208 ± 22 |
| Chenet al. | 3T | 3D IR-Cones Variable TR/TI | - | 131 + 12 | - |
| Reichert et al.(35) | 1.5 T | 2D SR-UTE | - | - | 140 - 260 |
| Techawiboonwong.(18) | 3T | 2D SR-UTE | - | - | 398 ± 7 |
| Han et al. (36) | 3T | 3D UTE Variable Flip Angle | - | - | ~120 |
| Han et al. (37) | 3T | 3D UTE Actual Flip Angle | - | - | ~210 |
| Caoetal. (38) | 4.7 T | 3D UTE-VTR | - | - | ~3600 |
| Du etal. (32) | 3T | 2D SR-UTE | - | - | 223 + 11 |
| Rad et al. (19) | 3T | 3D Hybrid UTE with Two TRs | - | - | 302 ± 45 |
| Horchetal. (12) | 4.7 T | IR CPMG | ~1000 | ~350 | - |
| Horch et al. (25) | 4.7 T | IR CPMG | 551 + 120 | 357 + 10 | - |
| Seifert et al.(22) | 1.5 T | SR CPMG | 651 + 273 | 82.6 + 10.4 | - |
| Seifert et al.(22) | 3T | SR CPMG | 880 ± 281 | 145 + 25 | - |
| Seifert et al.(22) | 7T | SR CPMG | 1790 + 470 | 400 + 68 | - |
| Seifert et al.(22) | 9.4 T | SR CPMG | 1300 ± 370 | 358 ± 240 | - |
| Akbari et al.(33) | 1.5 T | 3D GRE Variable TR | 111 - 243 | - | - |
| Chen et al. (39) | 3T | 2D SR-UTE & IR-UTE | 527 + 28 | 116 + 6 | 243 ± 37 |

Note: $T_1^{TW}$, $T_1^{PW}$, and $T_1^{BW}$ values reported in the literature are also listed for comparison.

were largely comparable with these from the literature, especially these from NMR spectroscopy studies (22,25). Those results also suggest that both $T_1^{PW}$ and $T_1^{BW}$ have strong field dependence.

Figure 4 shows selected images of the tibial midshaft of a 33-year-old healthy volunteer using 3D dual echo Cones with variable TR and single-echo IR-Cones with variable TR/TI combinations. Cortical bone is barely visible with the 3D Cones sequence as a result of the high signal from surrounding long $T_2$ muscle and marrow fat. The 3D IR-Cones sequence efficiently suppressed signals from the surrounding long $T_2$ muscle and marrow fat, providing improved dynamic range for cortical bone with relatively high SNR of 22.1~72.8 (higher SNR for longer TR/TI). Fitting of the signal recovery curve shows a short $T_1^{TW}$ of 273 ± 13 ms for water (combined bound and pore water) in cortical bone with a TE of 32 μs, a $T_1^{PW}$ of 518 ± 36 ms for pore water in cortical bone with a TE of 2.5 ms. Fitting of the 3D IR-Cones images with different TR and TI combinations shows a $T_1^{BW}$ of 126 ± 8 ms for bound water in cortical bone. Fitting residues are typically less than 2% of the total signal, suggesting the effectiveness of the IR-Cones variable TR/TI approach in measuring $T_1^{BW}$. $T_1^{TW}$, $T_1^{PW}$, and $T_1^{BW}$ in the tibial midshafts of healthy volunteers are largely consistent with those obtained from bovine cortical bone samples.

Table 2 lists the mean and standard deviation of $T_1^{TW}$, $T_1^{PW}$, and $T_1^{BW}$ calculated from 3D dual-echo Cones acquisitions with variable TRs, as well as 3D single IR-Cones acquisitions with variable TR and TI combinations in healthy volunteers. On average, a mean $T_1^{TW}$ of 246 ± 32 ms, a mean $T_1^{PW}$ of 524 ± 46 ms, and a mean $T_1^{BW}$ of 134 ± 11 ms were observed for the tibial midshafts of the eight healthy volunteers. These values were again largely consistent with the values obtained from bovine cortical bone samples as given in Table 1.

## DISCUSSION

$T_1$ relaxation, also known as spin-lattice relaxation, describes the recovery of longitudinal magnetization after the application of a radiofrequency pulse. The mechanisms of $T_1$ relaxation in cortical bone are poorly understood, and for reasons not currently known, most recent studies suggest that $T_1$ of cortical bone (assuming a single $T_1$ component) is much shorter than that of long $T_2$ tissues, including muscle, liver, and gray and white matter (18–20,33). In five different healthy volunteers (mean age 29 years), we previously obtained a mean total water $T_1$ measurement of 223 ± 11 ms using a saturation recovery 2D-UTE technique, comparing closely to 246 ± 32 ms obtained with variable TR 3D-Cones in this study (33). Reichert et al used a saturation recovery technique and a 2D-UTE technique in vivo on a 1.5T system and found a range of 140–260 ms for $T_1$ measurement of total water (37). Rad et al employed a hybrid 3D UTE imaging with two different TRs approach to map $T_1$ and reported a total water $T_1$ of 302 ± 45 ms at 3 T (19). Using a saturation recovery technique and 3D-UTE imaging on a 3T scanner, Techawiboonwong et al found a mean total water $T_1$ of 398 ± 7 ms in human tibial cortex specimens (18). It is expected that the donor specimens used in their study (mean age at death of 67 years) would yield higher $T_1$ values than in our volunteers, as our volunteers were younger and presumably have lower cortical

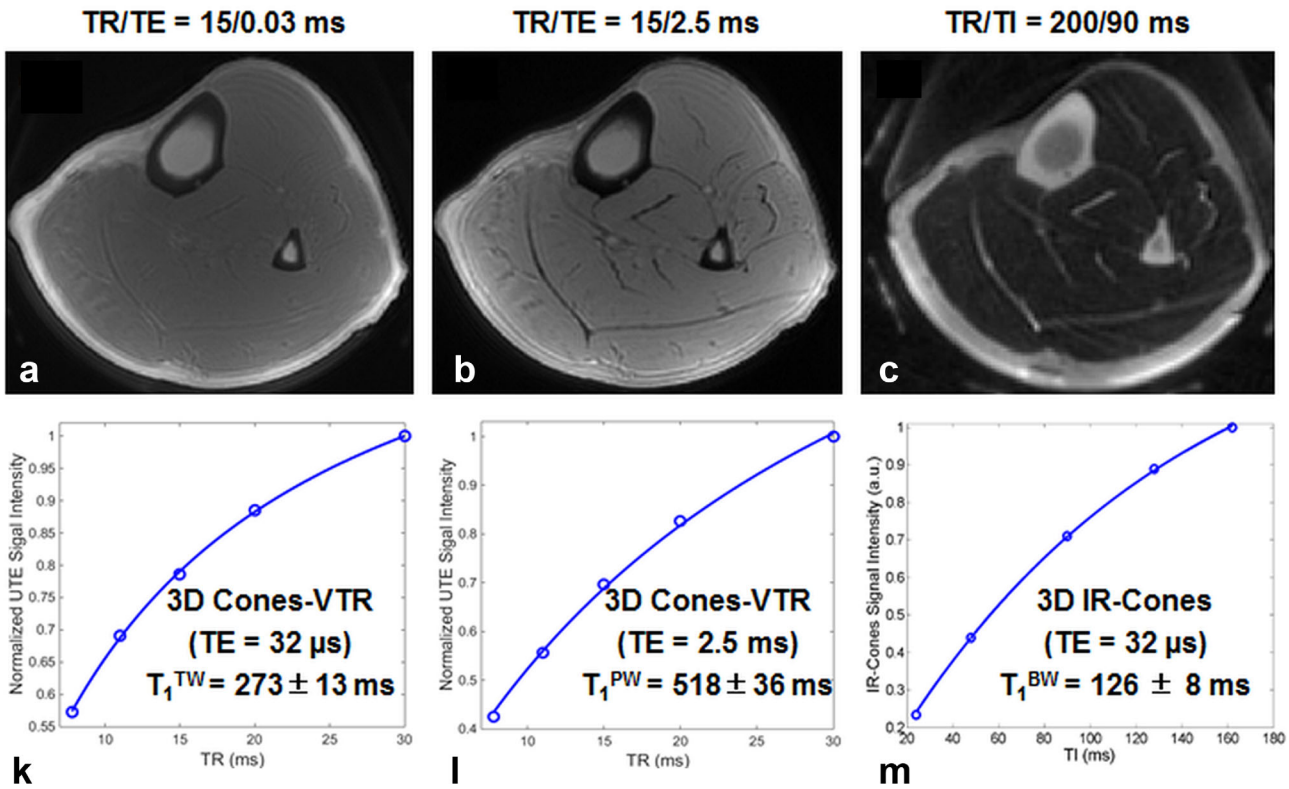


FIG. 4. Representative 3D dual echo Cones-VTR imaging of the tibial midshaft of a 33-year-old healthy volunteer with a TR of 15 ms, dual TEs of 32 μs (a) and 2.5 ms (b) in 2.5-min scan time, as well as 3D IR-Cones imaging with a TR of 200 ms and a TI of 90 ms in 2-min scan time (c). Single-component exponential recovery curve fitting of dual echo 3D Cones images with variable TRs shows a $T_1^{TW}$ of 273 ± 13 ms (d) and a $T_1^{PW}$ of 518 ± 36 ms (e), whereas the fitting of IR-Cones images with variable TR/TI combinations shows a $T_1^{BW}$ of 126 ± 8 ms (f) for cortical bone.

porosity than elderly specimens. More recently, Han et al investigated the temperature dependence of $T_1$ in cortical bone at 3 T using a varying flip angle approach (ie, 8° and 44°) and found that a linear relationship with $T_1$ increased from ~120 ms at 25.1 °C to ~155 ms at 70.1 °C (38). The same group also reported an actual flip angle imaging (AFI) UTE technique to improve $T_1$ measurement for short $T_2$ tissues, and reported a short $T_1$ value of ~210 ms for cortical bone at 3 T (39). The rapid $T_1$ relaxation of bone provides a unique opportunity, as quantification can potentially be performed without significantly prolonging imaging protocol. However, there are some studies suggesting that bone has a long $T_1$, instead of a short $T_1$. For example, Cao et al reported a very long $T_1$ of 3.6 s for cortical bone at 4.7 T (40). This result is consistent with the long $T_1$ values expected for solid-state materials. Clearly, more research is needed to further validate $T_1$ measurements of bone water using both high-performance NMR spectrometers as well as clinical MR scanners.

A number of recent studies have demonstrated that the different water components in cortical bone have very distinct $T_2$ and $T_2^*$ relaxation times. Pore water has a long $T_2$ ($>100$ ms) but a short $T_2^*$ (~a few milliseconds), whereas bound water has much reduced $T_2$ and $T_2^*$ (~a few hundred microseconds) (10–14,17). The distinct $T_2^*$ values suggest that the exchange rate between bound and pore water is relatively slow. As a result, one would also expect that bound and pore water should have distinct $T_1$ values. However, limited studies have been reported on this topic. Only a few groups to date have investigated techniques to measure $T_1$ values of bound and pore water in cortical bone. Using inversion recovery Carr-Purcell-Meiboom-Gill (CPMG) sequences and fitting with a 2D $T_1$-$T_2$ spectrum, Horch et al found shorter $T_1$ values of ~350 ms for bound water and ~1 s for pore water (12). In another study by the same group, a mean $T_1^{BW}$ of 357 ± 10 ms and a mean $T_1^{PW}$ of 551 ± 120 ms were reported for human cortical bone samples at 4.7 T (25). Chen et al reported a mean $T_1^{BW}$ of 116 ± 6 ms and a

Table 2
Measurement of $T_1$ Values of Pore Water ($T_1^{PW}$), Bound Water ($T_1^{BW}$), and Total Water ($T_1^{TW}$) in Tibial Midshaft of Healthy Volunteers (n = 8) Using 3D Dual Echo Cones With Variable TRs, and 3D IR-Cones With Variable TR and TI Combinations, Respectively.

| Sequences | Pore Water $T_1$, ($T_1^{PW}$, ms) | Bound Water $T_1$, ($T_1^{BW}$, ms) | Total Water $T_1$, ($T_1^{TW}$, ms) |
|---|---|---|---|
| 3D dual-echo Cones Variable TR | 524 + 46 | . | 246 + 32 |
| 3D IR-Cones Variable TR/TI | - | 134 ± 11 | - |

mean $T_1^{PW}$ of $527 \pm 28$ ms for bovine cortical bone samples at 3 T (41). Seifert et al reported a mean $T_1^{PW}$ of $880 \pm 281$ ms and a mean $T_1^{BW}$ of $145 \pm 25$ ms at 3 T (22). More recently, Akbari et al proposed the use of a clinical gradient echo sequence with a relatively short echo time of ~1.29 ms and variable TRs (ie, TR = 20 and 60 ms) to measure the $T_1$ of pore water. They reported a relatively short $T_1$ of 111–243 ms for the $T_1$ of pore water at 1.5 T (34). The $T_1^{BW}$ value from our study is very close to that reported by Seifert et al. Meanwhile, the mean $T_1^{PW}$ values of $880 \pm 281$ ms at 3 T and $1790 \pm 470$ ms at 7 T from the Seifert study are significantly higher than the mean $T_1^{PW}$ values of $545 \pm 28$ ms at 3 T from our study, $551 \pm 120$ ms at 4.7 T from the Horch study, and 111–243 ms at 1.5 T from the Akbari study. The variability may be the result of multiple factors, including differences in field strengths ($T_1$ is field strength dependent) and type of specimen ($T_1^{PW}$ in human cortical bone with larger pores is expected to be longer than in bovine cortical bone with smaller pores). More work is needed to validate the different techniques to measure $T_1^{PW}$ and $T_1^{BW}$.

In this study, we have demonstrated that the fast, volumetric 3D-Cones sequences provide additional opportunities for quantification, as ultrashort echo times can now be employed in a time and SNR-efficient manner. In bovine bone samples, the dual-echo variable TR 3D-Cones sequence produced similar results compared with the nonselective 2D UTE sequence using both dual-echo TSR and variable TR techniques for the quantification of total and bound water. For $T_1$ measurements of bound water, the IR technique using the 3D-Cones sequence yielded a mean measurement of 144 ms, compared with 116 ms obtained using the 2D-UTE sequence. This may be the result of the differences in spatial resolution, echo times, and sampling window. The 2D-UTE sequence with shorter echo time and sampling window is more efficient in capturing signal from a larger proportion of the rapidly decaying bound water component. Furthermore, the 2D UTE sequence is non-slice selective. $B_1$ variation across the specimen thickness (~6 cm) will also affect the $T_1$ measurement.

This study has a number of limitations. First, a single-component model was used for the $T_1$ calculation of total water, which is only an approximation. Multicomponent analysis would be helpful to elucidate the fractions and $T_1$ values of the bound and free water pools (22). However, the accuracy of multicomponent fitting is dependent on the quality of data including SNR, number of sampling points (or echo times), and separation of relaxation times. The 3D-Cones sequence may be well suited for multicomponent modeling, and this deserves additional study. Second, errors in $T_1^{PW}$ measurements would lead to imperfect nulling of pore water, resulting in long $T_2$ signal contamination in IR-UTE imaging of bound water, and thus errors in $T_1^{BW}$ estimation using the IR-Cones acquisitions with variable TR and TI combinations. Third, flip angle errors were not considered in the $T_1$ quantification in this study. $B_1$ mapping or actual flip angle imaging (AFI) techniques would likely improve the accuracy of $T_1^{TW}$, $T_1^{PW}$, and $T_1^{BW}$ measurements (39). Fourth, mapping of bound and pore water concentrations were not performed in this study. With $T_2^*$ and $T_1$ values of both bound and pore water components known, accurate measurement of their absolute concentration can be achieved easily through comparison of bone signal with that of a reference phantom with known proton density. Validation studies as well as clinical applications of total, bound, and pore water mapping will be performed in future studies.

## ACKNOWLEDGMENTS

The authors acknowledge the grant support from GE Healthcare, NIH (1R01 AR062581 and 1R01 AR068987) and the VA Clinical Science R&D Service (5IK2CX000749), as well as the International Postdoctoral Exchange Fellowship Program (No. 20130021) from China.

## REFERENCES

1. NIH Consensus Development Panel on Osteoporosis Prevention, Diagnosis, and Therapy, March 7-29, 2000: highlights of the conference. South Med J 2001;94:569–573.
2. Hahn M, Vogel M, Pompesius-Kempa M, Delling G. Trabecular bone pattern factor—a new parameter for simple quantification of bone microarchitecture. Bone 1992;13:327–330.
3. Bousson V, Peyrin F, Bergot C, Hausard M, Sautet A, Laredo JD. Cortical bone in the human femoral neck: three-dimensional appearance and porosity using synchrotron radiation. J Bone Miner Res 2004;19:794–801.
4. Bousson V, Bergot C, Meunier A, Barbot F, Parlier-Cuau C, Laval-Jeantet AM, Laredo JD. CT of the middiaphyseal femur: cortical bone mineral density and relation to porosity. Radiology 2000;217:179–187.
5. Pistoia W, van Rietbergen B, Ruegsegger P. Mechanical consequences of different scenarios for simulated bone atrophy and recovery in the distal radius. Bone 2003;33:937–945.
6. Zebaze RM, Ghasem-Zadeh A, Bohte A, Iuliano-Burns S, Mirams M, Price RI, Mackie EJ, Seeman E. Intracortical remodelling and porosity in the distal radius and post-mortem femurs of women: a cross-sectional study. Lancet 2010;375:1729–1736.
7. Ritchie RO, Buehler MJ, Hansma P. Plasticity and toughness in bone. Phys Today 2009;62:41–47.
8. Cowin SC. Bone poroelasticity. J Biomech 1999;32:217–238.
9. Wehrli FW, Song HK, Saha PK, Wright AC. Quantitative MRI for the assessment of bone structure and function. NMR Biomed 2006;19:731–764.
10. Wang XD, Ni QW. Determination of cortical bone porosity and pore size distribution using a low field pulsed NMR approach. J Orthop Res 2003;21:312–319.
11. Nyman JS, Ni Q, Nicolella DP, Wang X. Measurements of mobile and bound water by nuclear magnetic resonance correlate with mechanical properties of bone. Bone 2008;42:193–199.
12. Horch RA, Nyman JS, Gochberg DF, Dortch RD, Does MD. Characterization of 1H NMR signal in human cortical bone for magnetic resonance imaging. Magn Reson Med 2010;64:680–687.
13. Diaz E, Chung CB, Bae WC, Statum S, Znamirowski R, Bydder GM, Du J. Ultrashort echo time spectroscopic imaging (UTESI): an efficient method for quantifying bound and free water. NMR Biomed 2012;25:161–168.
14. Biswas R, Bae W, Diaz E, Masuda K, Chung CB, Bydder GM, Du J. Ultrashort echo time (UTE) imaging with bi-component analysis: bound and free water evaluation of bovine cortical bone subject to sequential drying. Bone 2012;50:749–755.
15. Horch RA, Gochberg DF, Nyman JS, Does MD. Non-invasive predictors of human cortical bone mechanical properties: T(2)-discriminated H NMR compared with high resolution X-ray. PLoS One 2011;6:e16359.
16. Bae WC, Chen PC, Chung CB, Masuda K, D'Lima D, Du J. Quantitative ultrashort echo time (UTE) MRI of human cortical bone: correlation with porosity and biomechanical properties. J Bone Miner Res 2012;27:848–857.

17. Du J, Hermida JC, Diaz E, Corbeil J, Znamirowski R, D'Lima DD, Bydder GM. Assessment of cortical bone with clinical and ultrashort echo time sequences. Magn Reson Med 2013;70:697–704.
18. Techawiboonwong A, Song HK, Leonard MB, Wehrli FW. Cortial bone water: in vivo quantification with ultrashort echo-time MR imaging. Radiology 2008;248:824–833.
19. Rad HS, Lam SCB, Magland JF, Ong H, Li C, Song HK, Love J, Wehrli FW. Quantifying cortical bone water in vivo by three-dimensional ultra-short echo time MRI. NMR Biomed 2011;24:855–864.
20. Li C, Seifert AC, Rad HS, Bhagat Y, Rajapakse CS, Sun W, Benny Lam SC, Wehrli FW. Cortical bone water concentration: dependence of MR imaging measures on age and pore volume fraction. Radiology 2014:272:796–806.
21. Du J, Diaz E, Carl M, Bae W, Chung C, Bydder GM. Ultrashort echo time imaging with bicomponent analysis. Magn Reson Med 2012;67:645–649.
22. Seifert AC, Wehrli SL, Wehrli FW. Bi-component T2* analysis of bound and pore bone water fractions fails at high field strengths. NMR Biomed 2015;28:861–872.
23. Rajapakse CS, Bashoor-Zadeh M, Li C, Sun W, Wright AC, Wehrli FW. Volumetric cortical bone porosity assessment with MR imaging: validation and clinical feasibility. Radiology 2015;19(5):141850.
24. Li S, Ma L, Chang E, Shao H, Chen J, Chung CB, Bydder GM, Du J. Effects of inversion time on inversion recovery prepared ultrashort echo time (IR-UTE) imaging of bound and pore water in cortical bone. NMR Biomed 2015;28:70–78.
25. Horch R, Gochberg D, Nyman J, Does M. Clinically-compatible MRI strategies for discriminating bound and pore water in cortical bone. Magn Reson Med 2012;68:1774–1784.
26. Manhard MK, Horch RA, Gochberg DF, Nyman JS, Does MD. In vivo quantitative MR imaging of bound and pore water in cortical bone. Radiology 2015;277:221–229.
27. Manhard MK, Horch RA, Harkins KD, Gochberg DF, Nyman JS, Does MD. Validation of quantitative bound- and pore-water imaging in cortical bone. Magn Reson Med 2014;71:2166–2171.
28. Gurney PT, Hargreaves BA, Nishimura DG. Design and analysis of a practical 3D cones trajectory. Magn Reson Med 2006;55:575–582.
29. Carl M, Bydder GM, Du J. UTE imaging with simultaneous water and fat signal suppression using a time-efficient multi-spoke inversion recovery pulse sequence. Magn Reson Med 2016;76:577–582.
30. Du J, Bydder M, Takahashi AM, Chung CB. Two-dimensional ultrashort echo time imaging using a spiral trajectory. Magn Reson Imaging 2008;26:304–312.
31. Tsai CM, Nishimura DG. Reduced aliasing artifacts using variable-density k-space sampling trajectories. Magn Reson Med 2000;43:452–458.
32. Wanspaura JP, Daniel BL, Pauly JM, Butts K. Temperature mapping of frozen tissue using eddy current compensated half excitation RF pulses. Magn Reson Med 2001;46:985–992.
33. Du J, Carl M, Bydder M, Takahashi A, Chung CB, Bydder GM. Qualitative and quantitative ultrashort echo time (UTE) imaging of cortical bone. J Magn Reson 2010;207:304–311.
34. Akbari A, Abbasi-Rad S, Rad HS. T1 correlates age: a short-TE MR relaxometry study in vivo on human cortical bone free water at 1.5T. Bone 2016;83:17–22.
35. Du J, Sheth V, He Q, Carl M, Chen J, Corey-Bloom J, Bydder GM. Measurement of T1 of the ultrashort T2* components in white matter of the brain at 3T. PLOS One 2014;e103296.
36. Larson PE, Conolly SM, Pauly JM, Nishimura DG. Using adiabatic inversion pulses for long-T2 suppression in ultrashort echo time (UTE) imaging. Magn Reson Med 2007;58:952–961.
37. Reichert ILH, Robson MD, Gatehouse PD, He T, Chappell KE, Holmes J, Girgis S, Bydder GM. Magnetic resonance imaging of cortical bone with ultrashort TE (UTE) pulse sequences. Magn Reson Imaging 2005;23:611–618.
38. Han M, Scott S, Ozhinsky E, Salgaonkar V, Jones P, Larson P, Diederich C, Krug R, Rieke V. Assessing temperature dependence of T1 in cortical bone using ultrashort echo-time MRI. J Therapy Ultrasound 2015;3(Suppl 1):P5.
39. Han M, Larson P, Krug R, Rieke V. Actual flip angle imaging to improve T1 measurement for short T2 tissues. In Proceedings of ISMRM 23rd Annual Meeting, Toronto, Canada, 2015. p. 501.
40. Cao H, Nazarian A, Ackerman JL, Snyder BD, Rosenberg AE, Nazarian RM, Hrovat MI, Dai G, Mintzopoulos D, Wu Y. Quantitative (31)P NMR spectroscopy and (1)H MRI measurements of bone mineral and matrix density differentiate metabolic bone diseases in rat models. Bone 2010;46:1582–1590.
41. Chen J, Grogan SP, Shao H, D'Lima D, Bydder GM, Wu Z, Du J. Evaluation of bound and pore water in cortical bone using ultrashort-TE MRI. NMR Biomed 2015;28:1754–1762.